nature medicine

Loss of BAP1 function leads to EZH2-dependent transformation

Lindsay M LaFave[1,2], Wendy Béguelin[3,15], Richard Koche[4,5,15], Matt Teater[3], Barbara Spitzer[6], Alan Chramiec[4], Efthymia Papalexi[1], Matthew D Keller[1], Todd Hricik[1], Katerina Konstantinoff[1], Jean-Baptiste Micol[1], Benjamin Durham[1], Sarah K Knutson[7], John E Campbell[7], Gil Blum[8,9], Xinxu Shi[10], Emma H Doud[11], Andrei V Krivtsov[4], Young Rock Chung[1], Inna Khodos[12], Elisa de Stanchina[12], Ouathek Ouerfelli[10], Prasad S Adusumilli[13], Paul M Thomas[11], Neil L Kelleher[11], Minkui Luo[8], Heike Keilhack[7], Omar Abdel-Wahab[1,14], Ari Melnick[3], Scott A Armstrong[4–6] & Ross L Levine[1,4,14]

The tumor suppressors BAP1 and ASXL1 interact to form a polycomb deubiquitinase complex that removes monoubiquitin from histone H2A lysine 119 (H2AK119Ub). However, *BAP1* and *ASXL1* are mutated in distinct cancer types, consistent with independent roles in regulating epigenetic state and malignant transformation. Here we demonstrate that *Bap1* loss in mice results in increased trimethylated histone H3 lysine 27 (H3K27me3), elevated enhancer of zeste 2 polycomb repressive complex 2 subunit (*Ezh2*) expression, and enhanced repression of polycomb repressive complex 2 (PRC2) targets. These findings contrast with the reduction in H3K27me3 levels seen with *Asxl1* loss. Conditional deletion of *Bap1* and *Ezh2 in vivo* abrogates the myeloid progenitor expansion induced by *Bap1* loss alone. Loss of BAP1 results in a marked decrease in H4K20 monomethylation (H4K20me1). Consistent with a role for H4K20me1 in the transcriptional regulation of EZH2, expression of SETD8—the H4K20me1 methyltransferase—reduces EZH2 expression and abrogates the proliferation of *BAP1*-mutant cells. Furthermore, mesothelioma cells that lack BAP1 are sensitive to EZH2 pharmacologic inhibition, suggesting a novel therapeutic approach for *BAP1*-mutant malignancies.

Genomic studies have identified somatic mutations in the tumor suppressors *ASXL1* and *BAP1* in different malignancies. Inactivating mutations in *ASXL1* are most common in myeloid malignancies[1–3], whereas recurrent *BAP1* mutations are commonly observed in mesothelioma[4], renal cell carcinoma[5] and metastatic uveal melanoma[6], which suggests that *BAP1* and *ASXL1* have distinct roles in tumor suppression. These mutational profiles cannot be explained by differential tissue-specific *BAP1* and *ASXL1* expression (**Supplementary Fig. 1a–c**). The *Drosophila* ASXL1 homolog Asx and the BAP1 homolog Calypso form a complex that removes H2AK119Ub (ref. 7). However, the BAP1–ASXL1 complex has not been shown to have a role in *BAP1*-mutant transformation. We sought to identify mechanisms by which BAP1 loss leads to transformation, independent of ASXL1 activity, and to identify therapeutic vulnerabilities in *BAP1*-mutant cancer cells.

Recent studies have shown that somatic loss of *Bap1* promotes hematopoietic transformation in mice[8]. We investigated the impact of conditional *Bap1* deletion on gene expression and chromatin state in hematopoietic cells (**Supplementary Fig. 1d**). *Bap1* loss led to a fully penetrant myeloproliferative disease with splenomegaly, leukocytosis, anemia and progenitor expansion (**Fig. 1a** and **Supplementary Fig. 1e–k**). We observed increased proliferation and cell cycle progression in *Bap1*-deficient myeloid progenitors (**Supplementary Fig. 1l**). RNA-sequencing analysis revealed that the majority of differentially expressed genes in *Bap1*-deficient progenitors had reduced expression (P adj. < 0.001) (**Supplementary Fig. 2a**). Although we observed significant overlap between differentially expressed genes in *Bap1*- and *Asxl1*-knockout (KO) progenitors[9], in many cases we observed a paradoxical inverse effect on gene expression (n = 714 genes overlap, 247 directly correlated, total n = 4,246 *Bap1*-KO, n = 1,761 *Asxl1*-KO) (**Fig. 1b** and **Supplementary Fig. 2b**). Silencing *ASXL1* leads to the increased expression of *HoxA* cluster genes, an observation that is consistent with reduced PRC2 activity[10]. However, we observed reduced expression of *HoxA* gene members (**Fig. 1c**) and decreased expression of *HoxA* gene

[1]Human Oncology and Pathogenesis Program, Memorial Sloan Kettering Cancer Center, New York, New York, USA. [2]Gerstner Sloan Kettering School of Biomedical Sciences, New York, New York, USA. [3]Department of Hematology/Oncology, Weill Cornell Medical College, New York, New York, USA. [4]The Center for Epigenetics Research, Memorial Sloan Kettering Cancer Center, New York, New York, USA. [5]Cancer Biology and Genetics Program, Memorial Sloan Kettering Cancer Center, New York, New York, USA. [6]Department of Pediatrics, Memorial Sloan Kettering Cancer Center, New York, New York, USA. [7]Epizyme, Inc., Cambridge, Massachusetts, USA. [8]Chemical Biology Program, Memorial Sloan Kettering Cancer Center, New York, New York, USA. [9]Tri-Institutional Program in Chemical Biology, Memorial Sloan Kettering Cancer Center, New York, New York, USA. [10]Chemical Synthesis Core, Memorial Sloan Kettering Cancer Center, New York, New York, USA. [11]Proteomics Center of Excellence, Northwestern University, Evanston, Illinois, USA. [12]Anti-Tumor Assessment Core, Memorial Sloan Kettering Cancer Center, New York, New York, USA. [13]Department of Surgery, Memorial Sloan Kettering Cancer Center, New York, New York, USA. [14]Leukemia Service, Department of Medicine, Memorial Sloan Kettering Cancer Center, New York, New York, USA. [15]These authors contributed equally to this work. Correspondence should be addressed to R.L.L. (leviner@mskcc.org).

Received 14 November 2014; accepted 19 August 2015; published online 5 October 2015; doi:10.1038/nm.3947

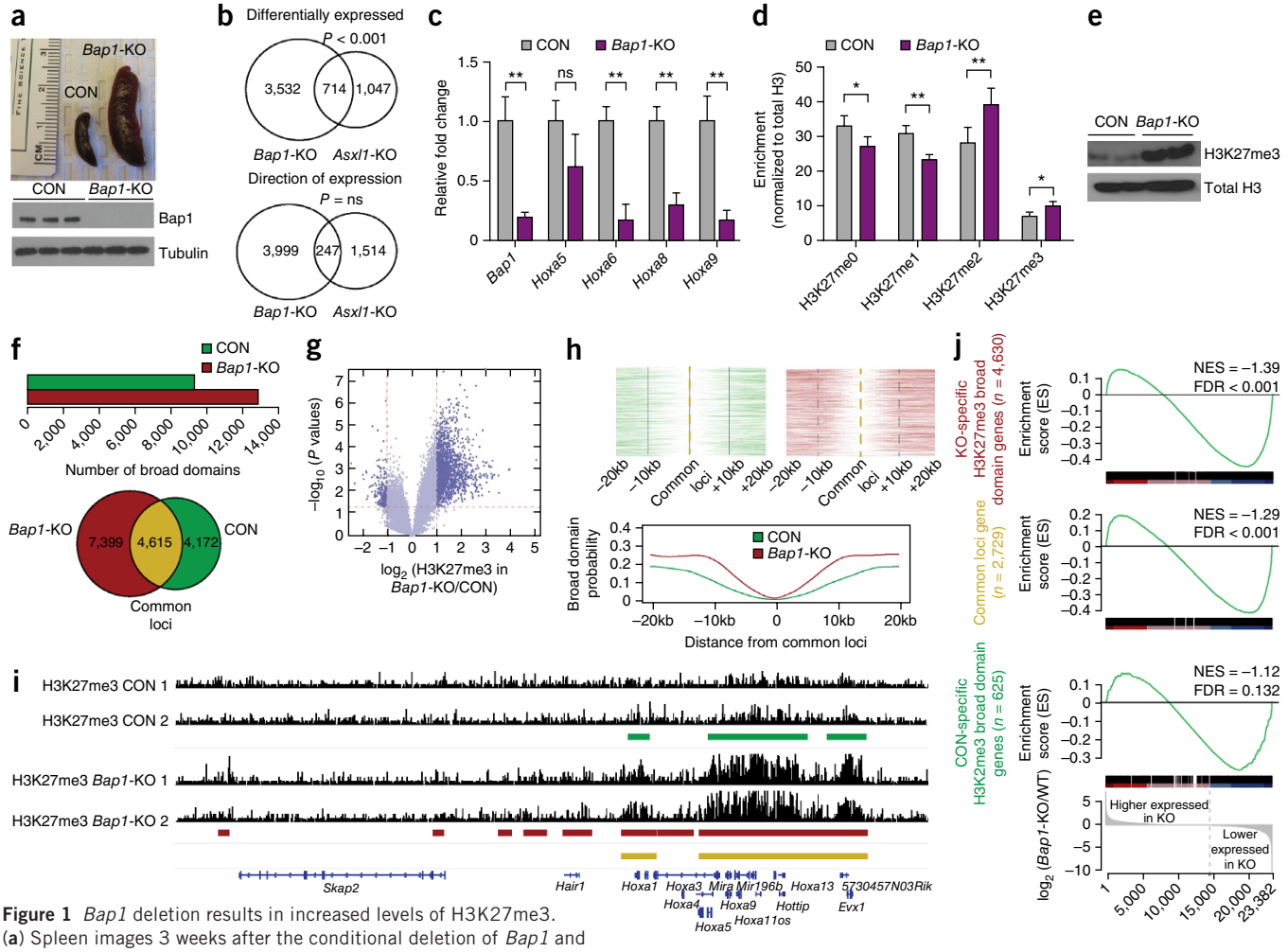

Figure 1 *Bap1* deletion results in increased levels of H3K27me3. (**a**) Spleen images 3 weeks after the conditional deletion of *Bap1* and verification of *Bap1* deletion by western blotting of control (littermate $Bap1^{f/f}$ mice, CON) and *Bap1*-KO (*Mx1-Cre* $Bap1^{f/f}$ mice) bone marrow. (**b**) Venn diagrams comparing myeloid progenitor gene expression in *Bap1*- and *Asxl1*-KO mice, $P < 0.05$; comparisons include gene overlap and genes changing in the same direction. (**c**) Quantitative real-time PCR (qRT-PCR) of the *HoxA* cluster in sorted granulocyte-macrophage progenitors (GMPs; $Lin^{-}c\text{-}Kit^{+}Sca1^{-}\ CD34^{+}\ Fc\gamma^{+}$); from *Bap1*-KO and control mice ($n = 3$). Relative fold change of genes in *Bap1*-KO mice compared to controls. (**d**) Mass spectrometric analysis of purified histones from $c\text{-}Kit^{+}$–enriched bone marrow cells from *Bap1*-KO mice and controls normalized to total histone H3. (**e**) Western blot of H3K27me3 and total H3 in purified histones from *Bap1*-KO and control bone marrow. (**f**) Number of H3K27me3 broad domains called in CON and *Bap1*-KO samples. Venn diagram showing unique and overlapping broad domains ($n = 2$). (**g**) Peak calls from H3K27me3 ChIP-seq in sorted GMP cells, represented by a volcano plot displayed by ratio (KO/CON) versus *P* value. (**h**) Broad domain density as a function of the distance from an H3K27me3 domain that was called in both CON and *Bap1*-KO samples. (**i**) H3K27me3 ChIP-seq at the *HOXA* locus. (**j**) Gene set enrichment analysis demonstrating gene expression correlations to downregulated genes. Statistics were calculated with Student's *t*-test; $^{*}P < 0.05$; $^{**}P < 0.005$; ns, not significant; error bars are means ± s.d.

signatures in *Bap1*-deficient cells (**Supplementary Fig. 2c**). These data demonstrate that the losses of *Asxl1* and *Bap1* have opposite effects on gene regulation.

ASXL1 directly interacts with the PRC2 complex and *ASXL1* deletion reduces levels of global and site-specific H3K27me3 (ref. 10). Given the divergent effects of *Asxl1* and *Bap1* loss on gene expression, we investigated the impact of *Bap1* deletion on H3K27me3. H3K27me3 levels were increased in *Bap1*-KO cells as measured by mass spectrometry, western blotting and ELISA (**Fig. 1d,e** and **Supplementary Fig. 3a**). Chromatin immunoprecipitation sequencing (ChIP-seq) revealed a global increase in H3K27me3 broad domains[11] and H3K27me3 'spreading' into nearby loci in *Bap1*-KO mice, as illustrated within the *HoxA* locus (**Fig. 1f–i** and **Supplementary Fig. 3b**). The sites marked with H3K27me3 in *Bap1*-KO cells primarily occurred in gene promoter regions (**Supplementary Fig. 3c**) that were enriched for enhanced repression (false discovery rate (FDR) < 0.001) (**Fig. 1j**). Genes dysregulated by *Bap1*-KO–associated H3K27me3 and gene repression were implicated in EZH2-dependent regulation, lineage commitment, differentiation and proliferation (**Supplementary Fig. 3d,e**). Silencing BAP1 increased H3K27me3 levels compared to controls. Re-expression of BAP1, but not a deubiquitinase-deficient BAP1 allele, in *Bap1*-KO cells reduced H3K27me3 levels compared to empty vector controls (**Supplementary Fig. 4a–c**).

We next assessed the role of PRC2-mediated H3K27me3 on BAP1-dependent transformation by investigating the impact of *Ezh2* loss[12] on transformation *in vivo*. *Ezh2* deletion reduced H3K27me3 levels in *Bap1*- and *Ezh2*-deficient mice as compared to *Bap1*-KO mice (**Fig. 2a**). *Ezh2* deletion abrogated the myeloid malignancy induced by *Bap1* loss, with reduced splenomegaly, leukocytosis and anemia

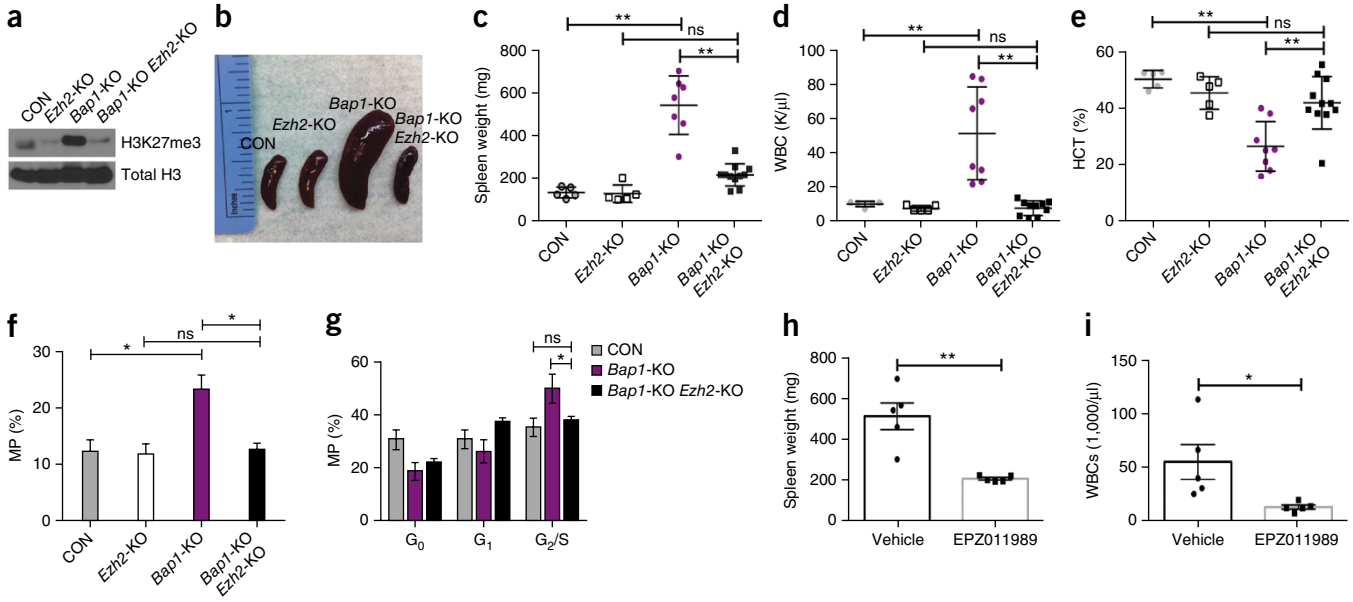

Figure 2 Proliferation induced by *Bap1* deletion is rescued by the loss of *Ezh2*. (**a**) Western blot of the H3K27me3 levels in histones purified from the bone marrow of *Bap1*-KO, *Ezh2*-KO, *Bap1*-KO and *Ezh2*-KO, and control mice. (**b**,**c**) Representative images of spleens (**b**) and enumeration of spleen weight (**c**) from the indicated genotypes of mice, 3 weeks after pIpC. (**d**,**e**) Peripheral white blood cell counts (**d**) and hematocrit percentages as quantified by a Hemavet (**e**). (**f**) Flow cytometric enumeration of myeloid progenitors (Lin$^-$c-Kit$^+$Sca1$^-$) ($n = 3$ per group). (**g**) Cell cycle analyses in myeloid progenitors using Ki67 and DAPI staining ($n = 3$ per group). (**h**,**i**) Spleen weights (**h**) and white blood cell (WBC) counts of mice ($n = 5$ per group) (**i**) treated with EPZ011989 or vehicle (0.5% NaCMC, sodium carboxymethyl cellulose + 0.1% Tween-80) twice a day at 500 mg per kg for 16 d. Unless otherwise indicated, $n = 5$ per CON, $n = 5$ per *Ezh2* KO, $n = 8$ per *Bap1* KO, and $n = 11$ per *Bap1/Ezh2* KO. Statistics were calculated with Student's *t*-test; $^*P < 0.05$; $^{**}P < 0.005$; ns, not significant; error bars show means ± s.d.

compared to *Bap1* deletion alone (**Fig. 2b–e** and **Supplementary Fig. 5a**). Concomitant *Bap1* and *Ezh2* loss reduced myeloid progenitor expansion, reduced the proportion of Mac1$^+$Gr1$^+$ myeloid cells, restored erythroid differentiation (CD71$^+$Ter119$^+$) and decreased the proliferation of *Bap1*- and *Ezh2*-deficient progenitors compared to cells with only *Bap1* deletion (**Fig. 2f–g** and **Supplementary Fig. 5b,c**).

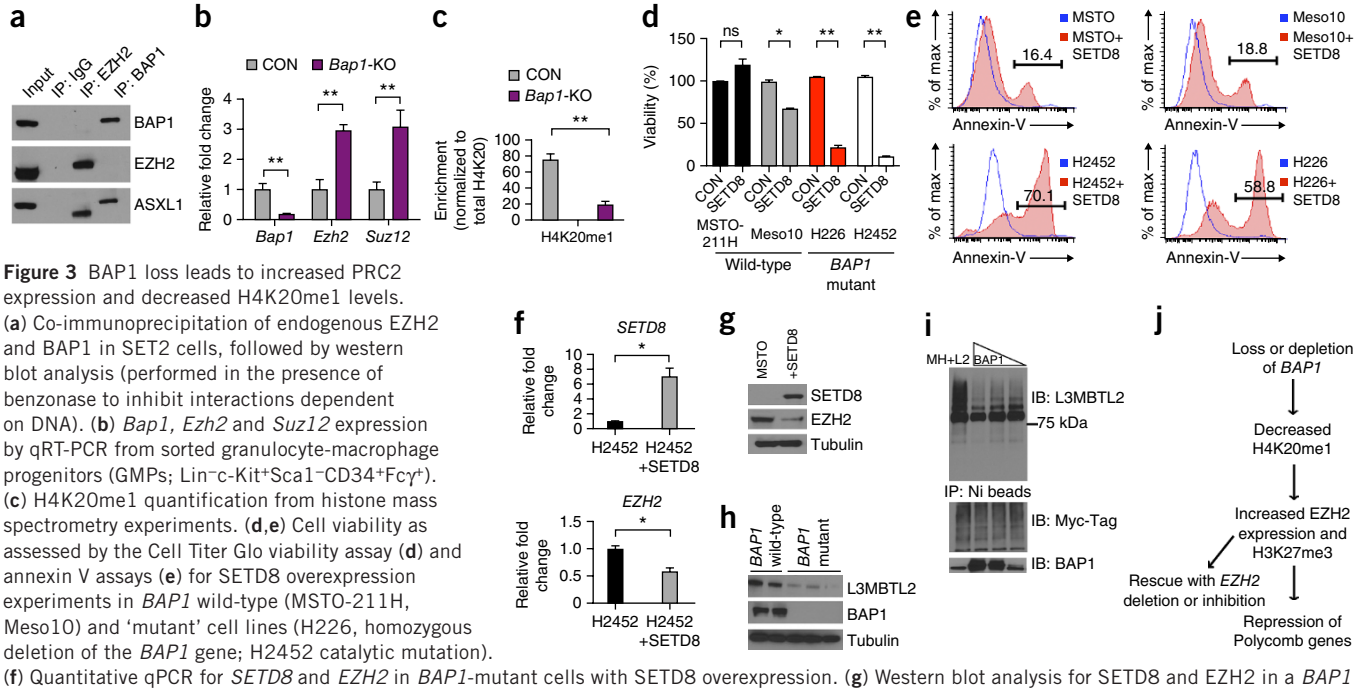

Figure 3 BAP1 loss leads to increased PRC2 expression and decreased H4K20me1 levels. (**a**) Co-immunoprecipitation of endogenous EZH2 and BAP1 in SET2 cells, followed by western blot analysis (performed in the presence of benzonase to inhibit interactions dependent on DNA). (**b**) *Bap1, Ezh2* and *Suz12* expression by qRT-PCR from sorted granulocyte-macrophage progenitors (GMPs; Lin$^-$c-Kit$^+$Sca1$^-$CD34$^+$Fcγ$^+$). (**c**) H4K20me1 quantification from histone mass spectrometry experiments. (**d**,**e**) Cell viability as assessed by the Cell Titer Glo viability assay (**d**) and annexin V assays (**e**) for SETD8 overexpression experiments in *BAP1* wild-type (MSTO-211H, Meso10) and 'mutant' cell lines (H226, homozygous deletion of the *BAP1* gene; H2452 catalytic mutation). (**f**) Quantitative qPCR for *SETD8* and *EZH2* in *BAP1*-mutant cells with SETD8 overexpression. (**g**) Western blot analysis for SETD8 and EZH2 in a *BAP1* wild-type cell line. (**h**) L3MBTL2 and BAP1 expression in *BAP1* wild-type (Met5a, JMN) and mutant mesothelioma cell lines (H226, H2452, H28). (**i**) 293T cells overexpressing Myc-His–tagged ubiquitin and L3MBTL2 cDNA and varying levels of BAP1 (0, 5 μg, 2.5 μg, 1 μg) from lanes left to right. Co-immunoprecipitation experiments were conducted with Ni-beads and a series of stringent washes. (**j**) Model depicting the regulation of *BAP1*, leading to effects on chromatin and gene expression. Statistics were calculated with Student's *t*-test; $^*P < 0.05$; $^{**}P < 0.005$; ns, not significant; error bars show means ± s.d.

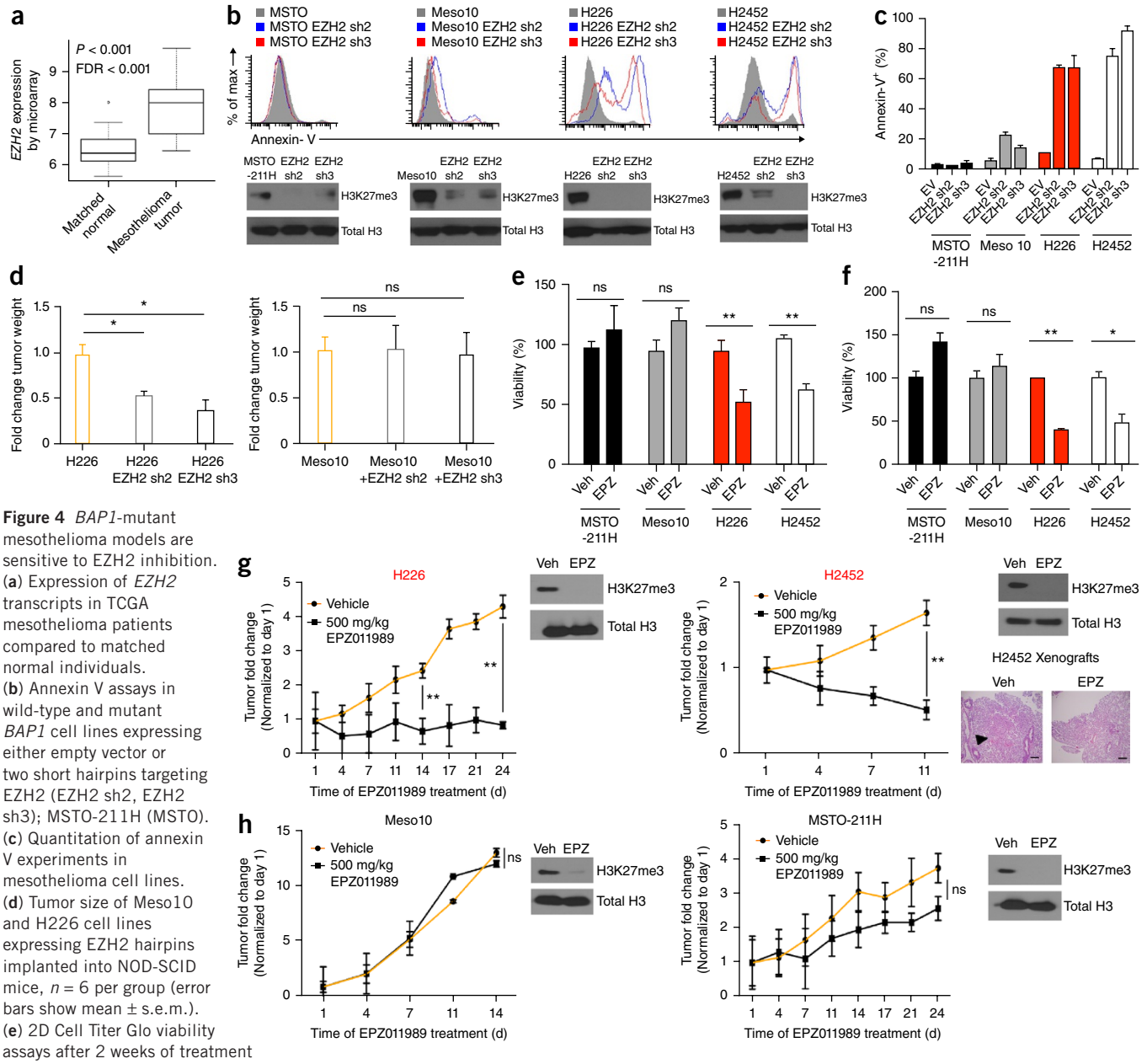

Figure 4 *BAP1*-mutant mesothelioma models are sensitive to EZH2 inhibition. (**a**) Expression of *EZH2* transcripts in TCGA mesothelioma patients compared to matched normal individuals. (**b**) Annexin V assays in wild-type and mutant *BAP1* cell lines expressing either empty vector or two short hairpins targeting EZH2 (EZH2 sh2, EZH2 sh3); MSTO-211H (MSTO). (**c**) Quantitation of annexin V experiments in mesothelioma cell lines. (**d**) Tumor size of Meso10 and H226 cell lines expressing EZH2 hairpins implanted into NOD-SCID mice, $n = 6$ per group (error bars show mean ± s.e.m.). (**e**) 2D Cell Titer Glo viability assays after 2 weeks of treatment with EPZ011989 at 1.25 μM. (**f**) 3D Cell Titer Glo viability assays after 5 d of EPZ011989 treatment at 1.25 μM. (**g**,**h**) Tumor-size formation from *BAP1*-mutant (H226 and H2452) (**g**) or wild-type cells (Meso10 and MSTO-211H) (**h**) implanted into NOD-SCID mice and treated with either vehicle or 500 mg/kg BID EPZ011989 (± s.e.m.). Tumors were measured 3× weekly, $n = 6$ per group. Target inhibition was assessed by histone western blots in extracted tumors (as shown). Lung pathology of H2452 cells with vehicle and EPZ011989 treatment is shown in **g**; magnification 100×; scale bars, 400 μm. Arrow indicates bulk metastasized tumor. Statistics were calculated with Student's *t*-test; $^*P < 0.05$; $^{**}P < 0.005$; ns, not significant; error bars show means ± s.d. unless otherwise indicated.

Consistent with the genetic data, treatment of *Bap1*-KO mice with the small-molecule EZH2 inhibitor EPZ011989 (ref. 13) decreased H3K27me3, splenomegaly and white blood cell counts compared to vehicle controls (**Fig. 2h,i** and **Supplementary Fig. 5d**). *Ezh2* haploinsufficiency reduced, but did not abrogate, *Bap1*-deficient myeloproliferation (**Supplementary Fig. 5e,f**), consistent with a dose-dependent requirement for *Ezh2*. These data demonstrate that *Ezh2* activity is required for *Bap1*-deficient myeloid transformation.

We next sought to delineate the mechanism by which *Bap1* deletion increased H3K27me3 levels. We did not identify an interaction between BAP1 and EZH2 by co-immunoprecipitation (**Fig. 3a**). We observed increased mRNA and protein expression of Ezh2 and Suz12, a canonical member of the PRC2 complex, consistent with a role for Bap1 in regulating PRC2 expression (**Fig. 3b** and **Supplementary Fig. 6a**). Re-expression of BAP1 in *Bap1*-KO bone marrow cells reduced *Ezh2* mRNA expression to normal levels (**Supplementary Fig. 6b**). We hypothesized that *Bap1* loss might alter other histone marks, which would then alter the chromatin state at key target loci, including EZH2. Mass spectrometry revealed a marked decrease in H4K20me1 levels in *Bap1*-KO cells (**Fig. 3c**) compared to other measured histone marks (**Supplementary Fig. 6c**). Expression of BAP1, but not of ASXL1, increased H4K20me1 at the *EZH2* locus (**Supplementary Fig. 6d**).

We therefore hypothesized that the loss of the H4K20me1 mark may have a role in BAP1-dependent gene expression. SETD8 is the only known methyltransferase that places H4K20me1 on chromatin[14]. The expression of SETD8 in *BAP1*-mutant mesothelioma cells (H226, H2452) increased apoptosis and reduced proliferation, whereas wild-type (MSTO-211H and Meso10) cells were unaffected (**Fig. 3d**,**e**). SETD8 overexpression in mesothelioma cells decreased EZH2 mRNA and protein expression compared to controls (**Fig. 3f**,**g**). Wild-type cell lines were more sensitive to the SETD8 inhibitor BVT594 (ref. 15) than were *BAP1*-mutant cell lines (**Supplementary Fig. 7a**).

We hypothesized that BAP1 deubiquitinates a chromatin modulator that regulates the levels of H4K20me1. Analysis of ChIP-seq data[8,9] identified a cluster of genes with BAP1 occupancy, but no ASXL1 binding, that were enriched for an E-box motif (**Supplementary Fig. 7b**,**c**). Previous studies have shown that the atypical polycomb proteins L3MBTL1 and L3MBTL2 bind E-box motifs and maintain H4K20me1 levels[16–19]. *L3mbtl1*-deficient mice exhibit no overt phenotype[20], whereas *L3mbtl2* deficiency is embryonic lethal at a rate similar to that of *Bap1* loss[8,17]. We therefore investigated whether *Bap1* loss leads to any alterations in L3mbtl2 expression. L3mbtl2 protein expression, but not RNA expression, was reduced in *Bap1*-KO hematopoietic cells (**Supplementary Fig. 8a**,**b**) and in *BAP1*-mutant mesothelioma cells, when compared to *BAP1* wild-type mesothelioma cells (**Fig. 3h**). L3MBTL2 ubiquitination was reduced in cells expressing BAP1 (**Fig. 3i**), and proteasome-inhibitor treatment increased L3MBTL2 stability in *BAP1*-mutant cells compared to controls (**Supplementary Fig. 8c**). L3MBTL2 expression decreased both EZH2 protein levels and EZH2 promoter activity (**Supplementary Fig. 8d**,**e**). Conversely, silencing L3MBTL2 led to an increase in the expression of EZH2 compared to that in the empty vector (**Supplementary Fig. 8f**). We observed enrichment for both L3MBTL2 and BAP1 at the *EZH2* locus (**Supplementary Fig. 8g**,**h**). These data suggest that BAP1 and L3MBTL2 interact (**Supplementary Fig. 8i**) and co-occupy the *EZH2* locus. *BAP1* loss leads to reduced L3MBTL2 stability and increased *EZH2* transcriptional output (**Fig. 3j**).

Analysis of The Cancer Genome Atlas (TCGA) data revealed that *EZH2* mRNA expression was increased in mesothelioma compared to matched normal tissue (**Fig. 4a**). Silencing EZH2 induced apoptosis in *BAP1*-mutant mesothelioma cell lines, whereas wild-type cells continued to proliferate (**Fig. 4b**,**c**). EZH2 silencing abrogated *in vivo* tumor formation of *BAP1*-mutant, but not of wild-type, cell lines (**Fig. 4d**). Overexpression of EZH2 increased proliferation and sensitivity of *BAP1* wild-type cell lines to EZH2 inhibition (**Supplementary Fig. 9a**,**b**). *BAP1*-mutant cell lines were more sensitive to EZH2 inhibition (EPZ011989) *in vitro* in 2D and 3D culture (**Fig. 4e**,**f**). We next assessed the effects of EZH2 inhibition *in vivo*. EZH2 inhibition significantly reduced tumor size in *BAP1*-mutant mice compared to vehicle-treated mice, whereas wild-type tumors were less responsive to EZH2 inhibition (**Fig. 4g**,**h**). EZH2 inhibition abrogated pulmonary metastasis in a *BAP1*-mutant mesothelioma cell line with metastatic potential (**Fig. 4g**), consistent with a role for BAP1 and EZH2 in metastasis[6]. EZH2 inhibition reduced the invasion H226 cells and increased E-cadherin expression *in vitro* compared to vehicle treatment. These data indicate that EZH2 represents a potential therapeutic target in *BAP1*-mutant cancer cells.

Identification of oncogenic *EZH2* mutations[21–23] led to the development of mutant-specific epigenetic therapies[24]. However, most mutations in epigenetic regulators result in a loss of function, such that they do not represent tractable direct therapeutic targets. EZH2 inhibitors have recently entered clinical trials (NCT01897571, NCT02395601, NCT02082977) and our data suggest that *BAP1* loss results in a mutation-specific dependency on PRC2 that should be further explored in preclinical and clinical studies. Our data resonate with recent studies suggesting a role for PRC2 inhibition in rhabdoid tumors with *SWI/SNF* remodeling complex mutations[25,26] and analyses showing that *BAP1* mutations are mutually exclusive with mutations in the *SWI/SNF* complex[27]. Our data suggest that studies of mutations in epigenetic regulators inform the development of therapies that reverse mutant-specific effects on epigenetic state.

METHODS

Methods and any associated references are available in the online version of the paper.

Accession codes. RNA-seq and ChIP-seq data are available via the GEO database, accession numbers GSE61577 and GSE61360, respectively.

Note: Any Supplementary Information and Source Data files are available in the online version of the paper.

ACKNOWLEDGMENTS

This work was supported by the Pershing Square Sohn Prize (R.L.L.), by grant 2R01GM096056 (M.L.), by grant CA172636 (R.L.L. and A.M.) and by grant F31 CA180642-02 (L.M.L.). Work in the Memorial Sloan Kettering Cancer Center (MSKCC) Core facilities that supported these studies is supported by P30 CA008748. R.L.L. is a Leukemia and Lymphoma Society Scholar. We would like to thank V. Rotter (Weizmann Institute of Science, Israel), X. Jiang (MSKCC), and M. Ladanyi (MSKCC) for generously providing plasmids for this work. We would like to thank D. Scheinberg (MSKCC) for generously sharing the mesothelioma cell lines used in this work.

AUTHOR CONTRIBUTIONS

L.M.L., O.A.-W. and R.L.L. designed the study. L.M.L., W.B., A.C., E.P., M.D.K., K.K., J.-B.M., I.K., E.H.D., X.S., Y.R.C. and O.A.-W. performed the experiments. L.M.L., W.B., R.K., M.T., B.S., T.H., A.C. and O.A.-W. performed ChIP-and RNA-Seq, sequencing and subsequent downstream analyses. B.D., S.K.K., J.E.C., G.B., E.d.S., O.O., P.S.A., P.M.T., N.L.K., M.L., H.K., A.M., S.A.A. and R.L.L. participated in data analysis and discussions. L.M.L. and R.L.L. prepared the manuscript with input from all authors.

COMPETING FINANCIAL INTERESTS

The authors declare competing financial interests: details are available in the online version of the paper.

1. Abdel-Wahab, O. *et al.* Concomitant analysis of *EZH2* and *ASXL1* mutations in myelofibrosis, chronic myelomonocytic leukemia and blast-phase myeloproliferative neoplasms. *Leukemia* **25**, 1200–1202 (2011).
2. Gelsi-Boyer, V. *et al.* Mutations of polycomb-associated gene *ASXL1* in myelodysplastic syndromes and chronic myelomonocytic leukaemia. *Br. J. Haematol.* **145**, 788–800 (2009).
3. Bejar, R. *et al.* Clinical effect of point mutations in myelodysplastic syndromes. *N. Engl. J. Med.* **364**, 2496–2506 (2011).
4. Bott, M. *et al.* The nuclear deubiquitinase BAP1 is commonly inactivated by somatic mutations and 3p21.1 losses in malignant pleural mesothelioma. *Nat. Genet.* **43**, 668–672 (2011).
5. Peña-Llopis, S. *et al.* BAP1 loss defines a new class of renal cell carcinoma. *Nat. Genet.* **44**, 751–759 (2012).
6. Harbour, J.W. *et al.* Frequent mutation of *BAP1* in metastasizing uveal melanomas. *Science* **330**, 1410–1413 (2010).
7. Scheuermann, J.C. *et al.* Histone H2A deubiquitinase activity of the polycomb repressive complex PR-DUB. *Nature* **465**, 243–247 (2010).
8. Dey, A. *et al.* Loss of the tumor suppressor BAP1 causes myeloid transformation. *Science* **337**, 1541–1546 (2012).
9. Abdel-Wahab, O. *et al.* Deletion of *Asxl1* results in myelodysplasia and severe developmental defects *in vivo*. *J. Exp. Med.* **210**, 2641–2659 (2013).
10. Abdel-Wahab, O. *et al.* *ASXL1* mutations promote myeloid transformation through loss of PRC2-mediated gene repression. *Cancer Cell* **22**, 180–193 (2012).
11. Béguelin, W. *et al.* EZH2 is required for germinal center formation and somatic EZH2 mutations promote lymphoid transformation. *Cancer Cell* **23**, 677–692 (2013).

12. Su, I.H. *et al. Ezh2* controls B cell development through histone H3 methylation and Igh rearrangement. *Nat. Immunol.* **4**, 124–131 (2003).
13. Campbell, J.E. *et al.* EPZ011989, a potent, orally available EZH2 inhibitor with robust *in vivo* activity. *ACS Med. Chem. Lett.* **6**, 491–495 (2015).
14. Nishioka, K. *et al.* PR-Set7 is a nucleosome-specific methyltransferase that modifies lysine 20 of histone H4 and is associated with silent chromatin. *Mol. Cell* **9**, 1201–1213 (2002).
15. Blum, G. *et al.* Small-molecule inhibitors of SETD8 with cellular activity. *ACS Chem. Biol.* **9**, 2471–2478 (2014).
16. Guo, Y. *et al.* Methylation-state-specific recognition of histones by the MBT repeat protein L3MBTL2. *Nucleic Acids Res.* **37**, 2204–2210 (2009).
17. Qin, J. *et al.* The polycomb group protein L3mbtl2 assembles an atypical PRC1-family complex that is essential in pluripotent stem cells and early development. *Cell Stem Cell* **11**, 319–332 (2012).
18. Trojer, P. *et al.* L3MBTL2 protein acts in concert with PcG protein-mediated monoubiquitination of H2A to establish a repressive chromatin structure. *Mol. Cell* **42**, 438–450 (2011).
19. Trojer, P. *et al.* L3MBTL1, a histone-methylation-dependent chromatin lock. *Cell* **129**, 915–928 (2007).
20. Qin, J. *et al.* Chromatin protein L3MBTL1 is dispensable for development and tumor suppression in mice. *J. Biol. Chem.* **285**, 27767–27775 (2010).
21. Morin, R.D. *et al.* Somatic mutations altering EZH2 (Tyr641) in follicular and diffuse large B-cell lymphomas of germinal-center origin. *Nat. Genet.* **42**, 181–185 (2010).
22. Morin, R.D. *et al.* Frequent mutation of histone-modifying genes in non-Hodgkin lymphoma. *Nature* **476**, 298–303 (2011).
23. Pasqualucci, L. *et al.* Analysis of the coding genome of diffuse large B-cell lymphoma. *Nat. Genet.* **43**, 830–837 (2011).
24. McCabe, M.T. *et al.* EZH2 inhibition as a therapeutic strategy for lymphoma with EZH2-activating mutations. *Nature* **492**, 108–112 (2012).
25. Knutson, S.K. *et al.* Durable tumor regression in genetically altered malignant rhabdoid tumors by inhibition of methyltransferase EZH2. *Proc. Natl. Acad. Sci. USA* **110**, 7922–7927 (2013).
26. Alimova, I. *et al.* Inhibition of EZH2 suppresses self-renewal and induces radiation sensitivity in atypical rhabdoid teratoid tumor cells. *Neuro-oncol.* **15**, 149–160 (2013).
27. Wilson, B.G. *et al.* Epigenetic antagonism between polycomb and SWI/SNF complexes during oncogenic transformation. *Cancer Cell* **18**, 316–328 (2010).

ONLINE METHODS

Animals. All animals were housed at the Memorial Sloan Kettering Cancer Center. All animal procedures were completed in accordance with the Guidelines for the Care and Use of Laboratory Animals and were approved by the Institutional Animal Care and Use Committees at the Memorial Sloan Kettering Cancer Center. The number of mice in each experiment was chosen to give 90% statistical power with a 5% error level, given the differences in s.d. that were observed in the pilot study.

Generation of *Bap1*-deficient and *Bap1*- and *Ezh2*-deficient mice. Embryonic stem cells targeting exons 6–12 of *Bap1* were obtained from the European Conditional Mouse Consortium. A *Frt*-flanked premature stop cassette containing a lacZ and neomycin cassette was inserted upstream[28]. ES cell clones were expanded and injected into primary blastocysts. Generated mice were crossed to the germline *Flp*-deleter (the Jackson Laboratory) to excise the *Frt*-flanked cassette. These mice were subsequently crossed with the IFN-α-inducible *Mx1-cre* transgenic mice (the Jackson Laboratory) to assess the effects of inducible loss of *Bap1* in the hematopoietic system. $Bap1^{fl/fl}$, $Bap1^{fl/+}$, and $Bap1^{+/+}$ littermate mice were genotyped by PCR with the primers BAP1-up (actgcagcaatgtggatctg), BAP1-down (gaaaaggtctgacccagatca) listed in 5′–3′ order using the following parameters: 95 °C for 10 min, followed by 40 cycles of 94 °C for 10 s, 65 °C for 40 s, and 72 °C for 1 min, and then 72 °C for 5 min. The WT allele was detected at 300 bp, and the floxed allele was detected at 500 bp by PCR. Excision after interferon (IFN)-α induction was confirmed by PCR with primers listed in 5′–3′ order to detect the floxed and excised band: BAP1-F (actgcagcaatgtggatctg), BAP1-F2 (gcgcaacgcaattaatgata) and BAP1-R (cagtgtccagaatggctcaa), using the same PCR parameters listed above.

Mx1-Cre-Bap1$^{f/f}$ mice were crossed with $Ezh2^{f/f}$ mice[29]. *Mx-cre Bap1*$^{f/f}$ conditional and $Bap1^{f/f}$ control mice received four intraperitoneal injections of polyI:polyC of 200 µl of a 1 mg per ml solution. Two weeks after excision, peripheral blood was collected via cheek bleeding using heparinized microhematocrit capillary tubes (Thermo Fisher Scientific). Excision was confirmed and peripheral blood counts were obtained using a HemaVet according to standard manufacturer's instructions. Formalin-fixed paraffin-embedded tissue sections were stained with H&E. The deletion of *Bap1* was confirmed by genomic excision PCR and western blot analysis. Tails were submitted to the Transnetyx genotyping service (Cordova, TN) for qPCR-based genotyping for floxed and excised *Ezh2* alleles. Excision was confirmed by western blot. Primer sequences are provided in **Supplementary Table 1**. No animals were excluded from genetic experiments.

Xenografts and *in vivo* EPZ011989 administration. Groups of 10-week-old NOD-SCID mice were injected subcutaneously in the flank with $6–10 \times 10^6$ cells from mesothelioma cell lines (MSTO-211H, Meso10, H226 and H2452) in a 1:1 mixture of Matrigel and media. When tumors reached a size of approximately 60–80 mm^3, we began treatment with either vehicle (0.5% NaCMC + 0.1% Tween-80 in water) or EPZ011989. Either EPZ011989 or the vehicle were given orally twice daily at a concentration of 500 mg per kg for the duration of the experiment. Tumor volumes were assessed in three dimensions using a caliper. Tumors or lung tissue were extracted following treatment and used for western blotting to assess target inhibition. We pre-established criteria to exclude mice in xenograft experiments if tumors did not form after implantation (defined as 75% smaller than the mean of the implanted animals from the same group). Animals were not excluded from drug trials. For all xenograft drug studies, tumor size was followed for 10 d and mice were randomized at this point for tumor size before the trial. The genetic *Bap1*-KO EPZ011989 trial was conducted with randomization using complete blood count (CBC) analysis 3 weeks after polyI:polyC and confirming that WBC count averages were equivalent in both the vehicle and treated groups. Five animals per group were treated orally with either vehicle (described above) or 500 mg per kg EPZ011989 twice daily for 16 d. Researchers were not blinded in these experiments.

Histological analyses. Mice were sacrificed and autopsied, and then dissected tissue samples were fixed for 24 h in 4% paraformaldehyde, dehydrated and embedded in paraffin. Paraffin blocks were sectioned at 4 µm and stained with H&E. Images were acquired using an Axio Observer A1 microscope (Carl Zeiss).

Cell culture. 293T cells were cultured in Dulbecco's modified Eagle's medium (DMEM) supplemented with 10% fetal bovine serum (FBS) and nonessential amino acids. Human leukemia cell lines (SET2) and human mesothelioma cell lines (Met5a, MSTO-211H, Meso10, H2373, H226, H2452) were cultured in RPMI-1640 medium supplemented with 10% FBS.

RNA isolation, SMARTer amplification, Proton transcriptome sequencing and analysis. Bone marrow cells were FACS-sorted for GMPs (Lin^-c-$Kit^+Sca1^-CD34^+Fc\gamma^+$) using the FACS Aria. Total RNA from 200,000–500,000 cells was extracted using TRIzol RNA Isolation Reagents (cat. no. 15596-026, Life Technologies). Quality of RNA was ensured before amplification by analyzing 20–50 pg of each sample using the RNA 6000 pico kit and a bioAnalyzer (Agilent). 10 ng of high quality (RNA integrity number (RIN) > 8) total RNA was subsequently amplified using the SMARTer Universal Low- Input RNA Kit for Sequencing (Clontech Laboratory, cat. no. 634940) according to the instructions provided by the manufacturer. Amplified material underwent whole-transcriptome library preparation according to the Ion Total RNA-seq Kit v2 protocol (Life Technologies), with 16 cycles of PCR. Samples were barcoded and template-positive Ion PI Ion Sphere Particles (ISPs) were prepared using the Ion One-Touch System II and Ion PI Template OT2 200kit v2 Kit (Life Technologies). Enriched particles were sequenced on a Proton sequencing system using 200-bp version 2 chemistry. An average of 70–80 million reads per sample were generated and 76–82% of the reads mapped to mRNA bases.

Raw output BAM files were converted back to FASTX format using PICARD Sam2Fastq (http://broadinstitute.github.io/picard/). The reads are first mapped to the mouse genome using rnaStar. The genome used was MM9 with junctions from Ensembl (Mus_musculus.NCBIM37.67) and a read overhang of 49. Then any unmapped reads were mapped to MM9 using the BWA-MEM algorithm (version 0.7.5a)[30]. The two mapped BAM files were then merged and sorted, and gene level counts were computed using htseq-count (options -s y -m intersection-strict) and the same gene models (Mus_musculus.NCBIM37.67). Raw data was uploaded to the Gene Expression Omnibus database with the following accession number: GSE61360.

Analyses of TCGA data in acute myeloid leukemia and mesothelioma. Average gene expression from TCGA acute myeloid leukemia patients was expressed as mathematical mean and standard error of normalized read counts as provided by DESeq2 (ref. 31). For TCGA mesothelioma patients, these same values were calculated from normalized read counts as provided by TCGA as level 3 data. To compare EZH2 expression of mesothelioma tumors to normal lung tissue[32], GSE51024 was analyzed using Geo2R, which makes use of the Limma Bioconductor R package. Normalized expression values for EZH2 were extracted from this analysis, and used to generate the box plots provided. Log_2 fold change, nominal *P* value, and Benjamini-Hochberg FDR were calculated by Geo2R/Limma.

Histone extraction, histone ELISAs, histone western blots and histone liquid chromatography–mass spectrometry (LC/MS). Histones were extracted by standard extraction techniques or overnight using the Active Motif Histone Extraction Minikit (cat. no. 40026). Histone ELISAs were conducted using the trimethyl K27 Elisa Kit (Active Motif, cat. no. 53106) normalized to a H3K27me3 standard curve and total H3 protein. Histone western blots were conducted with 3–5 µg of histones. For histone LC/MS, 12 million control and *Bap1*-KO cells were lysed, nuclei were isolated and histones were extracted using 0.4N H_2SO_4 and chemically derivatized using propionic anhydride, as previously described[33]. Histones were then digested with trypsin and separated by nano-liquid chromatography (75 µm i.d., 15 cm long, packed with MagicC18aq media, particle size 3 µm) coupled to a TSQ Quantum Ultra mass spectrometer. Data were analyzed with Skyline[34] and relative quantification was performed by peak area.

Chromatin preparation and immunoprecipitation, ChIP library preparation and sequencing and analysis of ChIP-seq data. Bone marrow cells were enriched for c-Kit^+ cells (or sorted for GMPs) using the EasySep Mouse Hematopoietic cell Enrichment Kit (Stem Cell Technologies, 19756). 5×10^6

doi:10.1038/nm.3947

cells were fixed in a 1% methanol-free formaldehyde solution and then resuspended in SDS lysis buffer. Lysates were sonicated in an E220 focused-ultrasonicator (Covaris) to a desired fragment size distribution of 100–500 base pairs. IP reactions were performed using anti-trimethyl H3K27 (Abcam, 6002), anti-monomethyl H4K20 (Abcam, 9051) and IgG (Santa Cruz, 2027) each on approximately 400,000 cells as previously described[35]. ChIP assays were processed on an SX-8G IP-STAR Compact Automated System (Diagenode) using a direct ChIP protocol as described elsewhere[36]. Eluted chromatin fragments were then de-crosslinked and the DNA fragments purified using Agencourt AMPure XP beads (Beckman Coulter).

Barcoded libraries were prepared from the ChIP-enriched and input DNA using a NEBNext ChIP-seq Library Prep Master Mix Set for Illumina (New England BioLabs) and TruSeq Adaptors (Illumina) according to the manufacturer's instructions on an SX-8G IP-STAR Compact Automated System (Diagenode). Phusion High-Fidelity DNA Polymerase (New England BioLabs) and TruSeq PCR Primers (Illumina) were used to amplify the libraries, which were then purified to remove adaptor dimers using AMPure XP beads and multiplexed on the HiSeq 2000 (Illumina).

Reads were quality and adapter-trimmed using 'trim_galore' before aligning to mouse assembly MM9 with Bowtie2 (ref. 37) using the default parameters. Aligned reads with the same start position and orientation were collapsed to a single read before subsequent analysis. Density profiles were created by extending each read to the average library fragment size and then computing density using the BEDTools suite[38]. For GMP sorted cells, enriched regions were discovered using MACS 1.4 with default parameters, and scored against matched input libraries. H3K27me3 broad domains were identified as described in Béguelin *et al.*[39]. Briefly, H3K27me3 ChIP-seq reads were calculated in 1 kb bins genome-wide. Enriched regions were binned consecutively with read counts greater than 1 s.d. of the genome-wide mean. Enriched regions were mapped to specific genomic locations: promoters, introns and exons, in addition to regions with specified distances from the transcription start site. All genome browser tracks and read density tables were normalized to sequencing depth. For comparison of ChIP-seq samples in control and KO conditions, the signals of three replicates per condition were tested using either the Mann-Whitney *U* test or the *t*-test. Cluster analysis was performed on normalized count data in MATLAB (the Mathworks) with the kmeans clustering package. Motif analysis was performed in Homer[40] using default parameters for the findMotifsGenome program.

Western blotting and immunoprecipitation. Cells were lysed for western blotting and immunoprecipitation experiments in the following buffer: 150 mM NaCl, 20 mM Tris (pH 7.4), 5 mM EDTA, 1% Triton X-100, protease arrest (EMD) and phosphatase inhibitors (Calbiochem). To perform immunoprecipitations in the presence of benzonase, cells were lysed in the BC-300 buffer: 20 mM Tris (pH 7.4), 10% glycerol, 300 mM KCl, 0.1% NP-40. The cleared lysate was treated with $MgCl_2$ to 2.5 mM and benzonase was added at 1250 U/mL. The lysate was incubated for 1 h with rotation and the reaction was terminated by adding 5 mM EDTA. DNA digestion was confirmed by running lysate on an ethidium bromide gel before setting up the immunoprecipitation experiment. Antibodies used included: BAP1 (C-4; Santa Cruz sc-28383; 1:1000), EZH2 (Active Motif, 39933, Active Motif, 39901, or Millipore, 07-689;1:10,000), SUZ12 (Abcam, Ab12073, 1:1000), ASXL1 (N-13; Santa Cruz sc-85283, 1:1000), L3MBTL2 (Active Motif, 39569, 1:1000), Myc-Tag (Cell Signaling, 2276; 1:2000), SETD8 (ab3798, 1:1000), Tubulin (Sigma, T9026, 1:10,000), H3K27me3 (Abcam, 6002 or Millipore, 07-449, 1:1000), H3 (Abcam, Ab1791, 1:10,000) and H4K20me1 (Abcam, Ab9051, 1:1000).

Flow cytometry analyses and antibodies. Surface marker staining of live bone marrow was conducted by first lysing cells with ammonium chloride–potassium bicarbonate lysis buffer and washing cells with phosphate-buffered saline (PBS). Cells were stained with antibodies in phosphate-buffered saline (PBS) for 20 min on ice. For hematopoietic stem and progenitor staining, cells were stained with a lineage cocktail including CD4 (clone RM4-5, BioLegend), CD3 (clone 17A2, BioLegend), B220 (clone RA3-6B2, BioLegend), NK1.1 (clone PK136, BioLegend), Gr-1 (clone RB6-8C5, BioLegend), Cd11b (clone M1/70, BioLegend) and Ter119 (cat no. 116223, BioLegend), allowing for mature lineage exclusion from the analysis. Cells were also stained with antibodies specific to c-Kit (clone 2B8, BioLegend), Sca-1 (clone D7, BioLegend), FcγRII/III (clone 2.4G2, eBiosciences) and CD34 (clone RAM34, eBiosciences) To assess the composition of the mature mononuclear cells we used Mac1, Gr-1, B220, and CD4/CD3. Cell-cycle analysis was conducted by staining cells with the hematopoietic stem and progenitor mix described above. Cells were fixed using the FIX and PERM kit (Invitrogen cat. no. GAS-003). Cells were stained with Ki67 after fixation and then stained with DAPI before analysis on the LSR Fortessa (BD Biosciences). Sorting was conducted by staining as described in text and above and utilization of a FACSAria sorter (BD Biosciences).

Plasmids. The cDNA full-length clone of human FLAG-L3MBTL2 was obtained from Addgene (Plasmid 28232). The cDNA human full-length clone of HA-FLAG BAP1 was obtained from Addgene (Plasmid 22539). Deubiquitinase mutant constructs (C91A, C91S) were generated using Agilent site-directed mutagenesis kits and confirmed by full-length DNA sequencing. Short-hairpin RNAs were obtained from the RNAi Consortium (TRC) in a pLKO.1 puromycin vector. Sequences for the short hairpins were as follows: human BAP1 (TRC Oligo IDs: TRCN0000007371 and TRCN0000007373), mouse BAP1 (TRCN0000030719 and TRCN0000030720), human L3MBTL2 (TRCN0000021724 and TRCN0000021726) and a control pLKO.1-puromycin vector encoding an shRNA for luciferase (shLUC).

Ubiquitin assays. HEK293T cells were seeded in a 10-cm dish and, 24 h later, were transduced with 4 μg of a Myc-His-Ubi expression construct and control, 1 μg L3MBTL2 and/or 1–10 μg BAP1-GFP overexpression constructs. Forty-eight hours after the transfection, cells were lysed in a Guanidine HCl–based lysis buffer: 6 M guanidine, 0.1 M NaH_2PO_4, 10 mM Tris, pH 8.0, and 10 mM BME. His-Ubi proteins were purified by incubation by 20 μL of Ni-NTA agarose (Qiagen) for 4 h at room temperature. Beads were washed sequentially with 1 mL of 4 wash buffers: buffer A 6 M guanidine, 0.1 M NaH_2PO_4, 10 mM Tris, pH 8.0, 10 mM BME, and 0.2% Triton X-100, buffer B 8 M urea, 0.1 M NaH_2PO_4, 10 mM Tris, pH 8.0, 10 mM BME, and 0.2% Triton X-100, buffer C 0.1 M NaH_2PO_4, 10 mM Tris, pH 6.3, 10 mM BME, and 0.2% Triton X-100, and buffer D 0.1 M NaH_2PO_4, 10 mM Tris, pH 6.3, 10 mM BME, and 0.1% Triton X-100. All buffers were supplemented with 15 mM imidazole. His-tagged proteins were purified from the beads by boiling with 2× SDS Laemmli buffer supplemented with imidazole. Proteins were then analyzed by western blot.

***In vitro* colony-forming assays.** Cells were sorted for $Lin^-c\text{-}Kit^+Sca1^+$ cells using the FACSAria. 100 cells were plated in duplicate in methylcellulose (MethoCult GF M3434, Stem Cell Technologies). Colonies were counted 14 d after plating, and colonies were collected by washing with PBS. Cells were then lysed for RNA and histone extraction.

Transient transfection. 293T cells were transfected with indicated constructs with X-treme gene transfection reagent (Roche). Protein and/or histones were extracted 48–72 h after transfection.

Invasion assays. Mesothelioma cells (MSTO-211H, H2373, H226 and H2452) were seeded in T75 flasks (100,000 cells). 12 h later, the plated cells were treated with GSK126 (0–2 μM) (Chemitek) and then left to proliferate for 7 d. 250,000 treated cells were then placed on the top of a Matrigel invasion chamber (BD Biosciences, cat no. 354480) in serum-free media, while the lower chamber contained media with serum. 22 h later, the cells on the bottom of the membrane were stained with crystal violet and quantified with ImageJ software from the US National Institutes of Health (NIH).

Luciferase assays. 293T cells were transiently transfected with the pGL3 EZH2 promoter reporter construct and a Switchgear *Renilla* control construct in addition to EV, BAP1, and L3MBTL2 constructs. Cells were assessed for luciferase activity using the Dual Luciferase Reporter Assay System (Promega). Cells were seeded in 24 well plates and were co-transfected with 200 ng of pGL3-EZH2-Luciferase, 200 ng of the *Renilla* luciferase control construct and 500 ng of experimental constructs. Cells were incubated 48 h after the transfection, lysed for 15 min at room temperature and luciferase activity was

assessed on a luminometer. The firefly luciferase readings were normalized to the *Renilla* transfection control.

Cell Titer Glo viability assays. Adherent mesothelioma cell lines were plated in 96 well dishes at about 100 cells per well to allow space for cells to proliferate. Cells were plated and given 1 d to adhere (an initial day 1 reading was taken at this time). ATP luminescence readings were taken at times specified in the manuscript. For the assays in which we assessed response to EPZ001989, the drug was added on day 1 and then replenished every 4 d.

Apoptosis assays. For apoptosis analysis, 1×10^6 cells were stained using the Annexin V–FITC apoptosis detection kit (BD) according to the manufacturer's recommendations. DAP1 was used as a counterstain in these experiments and heat-shock controls were used as positive controls.

3D-growth assays. To perform 3D assays in these cell lines, we used the technique using poly-HEMA as published for mesothelioma cell lines[41]. We prepared plates and spheroids as described with cells that had been pre-treated for 4 d with 500 nM EPZ011989. 5 d after treatment, we assessed viability using Cell Titer Glo assays.

Statistical analyses. The Student's *t*-test was used to analyze statistical significance unless described in the text. Normality tests were used to test the assumption of a normal distribution. Prism GraphPad Software was used for statistical calculations. Error was calculated using s.d. unless otherwise noted; $^*P < 0.05$, $^{**}P < 0.005$.

Replicates. c-Kit enrichment ChIP-seq experiments were conducted with four biological replicates, with two replicates combined for sequencing. GMP ChIP-seq experiments were conducted with three replicates for each group. c-Kit and GMP RNA-seq was conducted with three biological replicates from each group. Histone mass spectrometry experiments were conducted with three biological and three technical replicates. Genetic phenotyping experiments were replicated three times independently. Flow cytometric experiments were replicated independently two or three times. Pilot studies were conducted with drug studies and results were replicated in a larger study to achieve enough statistical power. *In vitro* experiments were replicated two or three times, with viability experiments being completed in triplicate.

28. Skarnes, W.C. *et al.* A conditional knockout resource for the genome-wide study of mouse gene function. *Nature* **474**, 337–342 (2011).
29. Su, I.H. *et al.* Ezh2 controls B cell development through histone H3 methylation and Igh rearrangement. *Nature immunology* **4**, 124–131 (2003).
30. Li, H. Aligning sequence reads, clone sequences and assembly contigs with BWA-MEM. arXiv:1303.3997v1 [q-bio.GN] (2013).
31. Love, M.I., Huber, W. & Anders, S. Moderated estimation of fold change and dispersion for RNA-seq data with DESeq2. *Genome Biol.* **15**, 550 (2014).
32. Suraokar, M.B. *et al.* Expression profiling stratifies mesothelioma tumors and signifies deregulation of spindle checkpoint pathway and microtubule network with therapeutic implications. *Ann. Oncol.* **25**, 1184–1192 (2014).
33. Garcia, B.A. *et al.* Chemical derivatization of histones for facilitated analysis by mass spectrometry. *Nat. Protoc.* **2**, 933–938 (2007).
34. MacLean, B. *et al.* Skyline: an open source document editor for creating and analyzing targeted proteomics experiments. *Bioinformatics* **26**, 966–968 (2010).
35. Krivtsov, A.V. *et al.* H3K79 methylation profiles define murine and human MLL-AF4 leukemias. *Cancer Cell* **14**, 355–368 (2008).
36. O'Geen, H., Echipare, L. & Farnham, P.J. Using ChIP-seq technology to generate high-resolution profiles of histone modifications. *Methods Mol. Biol.* **791**, 265–286 (2011).
37. Langmead, B. & Salzberg, S. Fast gapped-read alignment with Bowtie 2. *Nat. Methods* **9**, 357–359 (2012).
38. Quinlan, A.R. & Hall, I. M. BEDTools: a flexible suite of utilities for comparing genomic features. *Bioinformatics* **26**, 841–842 (2010).
39. Béguelin, W. *et al.* EZH2 is required for germinal center formation and somatic EZH2 mutations promote lymphoid transformation. *Cancer Cell* **23**, 677–692 (2013).
40. Heinz, S. *et al.* Simple combinations of lineage-Determining transcription factors prime cis-regulatory elements required for macrophage and B cell identities. *Mol. Cell* **38**, 576–589 (2010).
41. Phung, Y.T., Barbone, D., Broaddus, V.C. & Ho, M. Rapid generation of *in vitro* multicellular spheroids for the study of monoclonal antibody therapy. *J. Cancer* **2**, 507–514 (2011).

doi:10.1038/nm.3947